ACS Macro Letters

Letter

pubs.acs.org/macroletters

Polymerization-Induced Self-Assembly Using Visible Light Mediated Photoinduced Electron Transfer–Reversible Addition–Fragmentation Chain Transfer Polymerization

Jonathan Yeow, Jiangtao Xu, and Cyrille Boyer*

Centre for Advanced Macromolecular Design (CAMD) and Australian Centre for NanoMedicine (ACN), School of Chemical Engineering, UNSW Australia, Sydney, NSW 2052, Australia

Supporting Information

ABSTRACT: The ruthenium-based photoredox catalyst, $Ru(bpy)_3Cl_2$, was employed to activate reversible addition–fragmentation chain transfer (RAFT) dispersion polymerization via a photoinduced electron transfer (PET) process under visible light (λ = 460 nm, 0.7 mW/cm^2). Poly(oligo(ethylene glycol) methyl ether methacrylate) was chain extended with benzyl methacrylate to afford in situ self-assembled polymeric nanoparticles with various morphologies. The effect of different intrinsic reaction parameters, such as catalyst concentration, total solids content, and cosolvent addition was investigated with respect to the formation of different nanoparticle morphologies, including spherical micelles, worm-like micelles, and vesicles. Importantly, highly pure worm-like micelles were readily isolated due to the in situ formation of highly viscous gels. Finally, "ON/OFF" control over the dispersion polymerization was demonstrated by online Fourier transform near-infrared (FTNIR) spectroscopy, allowing for temporal control over the nanoparticle morphology.

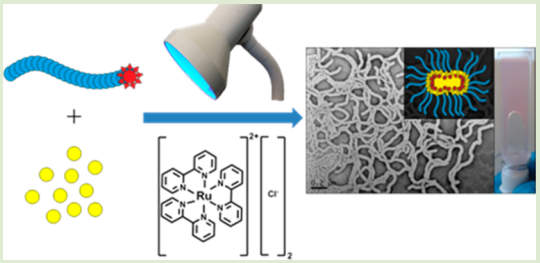

Nonspherical colloidal nanoparticles with diverse morphologies are of particular interest for applications in coatings, stabilizers, and drug delivery.[1] In the last few decades, the syntheses of nonspherical nanoparticles have been developed by direct self-assembly of block copolymers in selective solvents.[1b,2] However, generally the production of these materials is limited by the practical scalability and ability to reproducibly generate highly pure phases.[3] In the case of "intermediate" morphologies such as worm-like micelles, developing a reproducible synthesis is particularly challenging due to the narrow range of parameters needed to generate this morphology.[4] Furthermore, the self-assembly of amphiphilic block copolymers is typically performed using a multistep approach, ultimately yielding very dilute nanoparticle solutions (generally <1 wt %).[1b,3,5] The polymerization-induced self-assembly (PISA) process overcomes some of these limitations by utilizing the living polymerization of a solvophobic polymer to drive self-assembly in situ. In this way, polymeric nanoparticles can be produced at much higher solids content without the need for purification of preformed amphiphilic block copolymers. Extensive studies by Armes, Pan and others[4c,6] have demonstrated the ability of reversible addition–fragmentation chain transfer (RAFT) dispersion polymerization to generate a range of morphologies using a variety of monomer/solvent systems. Typically, these polymerizations are carried out using thermally activated radical sources, such as α,α'-azobis(isobutyronitrile) (AIBN) to initiate the polymerization. As a result, the nanoparticle morphologies are formed at elevated temperature before quenching to room temperature. In one approach, the polymerization of thermoresponsive polymers above the lower critical solution temperature (LCST) has been used to produce different nanoparticle morphologies that require cross-linking to prevent dissolution upon cooling, as demonstrated by Sumerlin, Charleux, and Hawker's groups.[6k,7] Interestingly, there have been limited reports of PISA-derived nanoparticles synthesized at room temperature.[8]

Yoshida reported a room temperature photoinitiated nitroxide-mediated polymerization, which was used to generate nano/microparticles in situ by chain extension of a poly(methacrylic acid) macroinitiator with a mixture of methyl methacrylate and methacrylic acid in a water–ethanol solvent system.[9] However, high energy UV light (500 W source) is required to initiate the polymerization and the results indicate limited control over particle uniformity. More recently, spherical particles such as poly(methyl methacrylate) microspheres[10] or poly(4-vinylpyridine)-*b*-poly(styrene) micelles[11] were produced at room temperature using slightly lower energy UV light (λ = 365 nm) in the presence of a photoinitiator using RAFT dispersion polymerization. In order to circumvent the issues associated with the use of UV light (e.g., monomer self-initiation and RAFT end group degradation), the use of visible light to mediate living polymerization was recently developed.[12] Significant advances have been made in the application of photoredox catalysts for controlling atom transfer radical

Received: July 28, 2015
Accepted: August 17, 2015
Published: August 27, 2015

ACS Publications © 2015 American Chemical Society

DOI: 10.1021/acsmacrolett.5b00523
ACS Macro Lett. 2015, 4, 984–990

Scheme 1. (A) Synthetic Approach for Producing Diblock Copolymer via PISA PET-RAFT Polymerization; (B) Proposed PET-RAFT Polymerization Mechanism

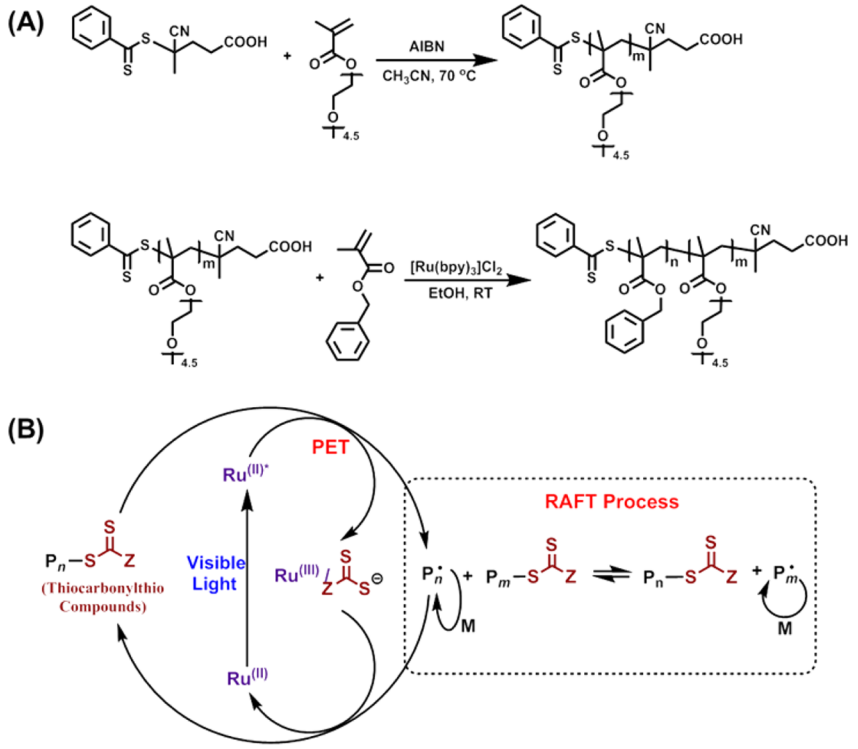

polymerization (ATRP),[13] ring-opening metathesis polymerization (ROMP),[14] and RAFT polymerizations.[15]

In this study, we report the first photoredox-catalyzed PISA approach for the preparation of various nanoparticle shapes. In this approach, we combine our recently developed living radical polymerization technique, photoinduced electron transfer-reversible addition−fragmentation chain transfer (PET-RAFT)[15a,d,16] polymerization with a PISA process. The ruthenium-based photoredox catalyst, $Ru(bpy)_3Cl_2$, was able to regulate the dispersion polymerization of benzyl methacrylate (BzMA) in ethanol (EtOH) using a poly(oligo(ethylene glycol) methyl ether methacrylate) (POEGMA) macro-chain transfer agent (macro-CTA) under blue light irradiation (λ_{max} = 460 nm, 0.7 mW/cm^2). In situ self-assembled nanoparticles with different morphologies, such as spherical micelles, worm-like micelles, and vesicles, were produced. It should be emphasized that pure worm-like micelles were readily isolated due to the formation of a physical gel. In addition, external temporal regulation by light was demonstrated by "ON/OFF" experiments. To the best of our knowledge, this study is the first report of a PISA polymerization mediated by visible light yielding non-spherical morphologies.

A POEGMA homopolymer ($M_{n,NMR}$ = 9000 g mol^{-1} and M_w/M_n = 1.10, SI, Figure S1 and Table S1), used as a macro-CTA, was synthesized via homogeneous RAFT polymerization (Scheme 1A). The molecular weight of the macro-CTA employed as a stabilizer block was carefully chosen. Indeed, if the stabilizer block is too long, restricted morphologies such as large compound micelles tend to form, but if it is too short, colloidal stability of the nanoparticles cannot be maintained. In order to initiate the PISA process, the POEGMA macro-CTA was then chain extended with BzMA, which is known to readily undergo controlled dispersion polymerization in ethanolic solution. Use of this methacrylic monomer is preferred over other systems such as styrene (in alcohols) since it possesses a significantly faster radical polymerization rate compared to styrene.[17] We have previously demonstrated the ability of photoredox catalysts to mediate PET-RAFT polymerizations (Scheme 1B) with good control over the molecular weight and molecular weight distributions.[15a,18] In this work, we selected the ruthenium complex, $Ru(bpy)_3Cl_2$ as photoredox catalyst, due to its good solubility in alcohols (Figure 1D).[19]

The catalytic efficiency of $Ru(bpy)_3Cl_2$ in polymerizing BzMA from the POEGMA macro-CTA was investigated using three different catalyst concentrations (20, 40, and 100 ppm relative to monomer concentration) with a [BzMA]/[POEGMA] = 200:1. Reaction vessels were irradiated with blue light (λ_{max} = 460 nm, 0.7 mW/cm^2) for 24 h before quenching the polymerizations. ^{1}H NMR indicated that monomer conversions gradually increased with catalyst concentration (Figure 1A). Successful chain extensions were further confirmed with ^{1}H NMR spectra of the purified diblock copolymers revealing the presence of characteristic methylene peaks (adjacent to ester) for PBzMA at δ 4.7−5.0 ppm and POEGMA at δ 3.9−4.1 ppm (SI, Figure S2A). At each catalyst concentration, the theoretical and experimental molecular weight values determined by NMR were in good agreement (Figure 1A). Gel permeation chromatography (GPC) traces indicated a controlled polymerization with relatively low dispersity (M_w/M_n < 1.25, Figure 1A,C). Using dual RI and UV (λ = 305 nm) detectors, high molecular weight shoulders can be clearly observed in GPC traces, which was attributed to bimolecular termination, as reported in several PISA formulations (SI, Figure S3).[6g,20] Furthermore, we observed a shoulder at low retention time, which is attributed to the presence of "unreacted" or "dead" chains. GPC deconvolution (SI, Figure S4) using a previous method reported in the literature,[21] gives around 10% of "unreacted" polymers. Part of

DOI: 10.1021/acsmacrolett.5b00523
ACS Macro Lett. 2015, 4, 984−990

(A)

Exp.	Catalyst (ppm)	Conversion (%)	$M_{n,\,theo}$ (g/mol)	$M_{n,\,NMR}$ (g/mol)	$M_{n,\,GPC}$ (g/mol)	Đ	D_h (DLS) (nm)	PDI (DLS)
i	20	41	23 400	24 100	16 800	1.19	46	0.13
ii	40	50	26 600	25 900	19 600	1.21	134	0.20
iii	100	61	30 500	28 600	22 600	1.24	140	0.17

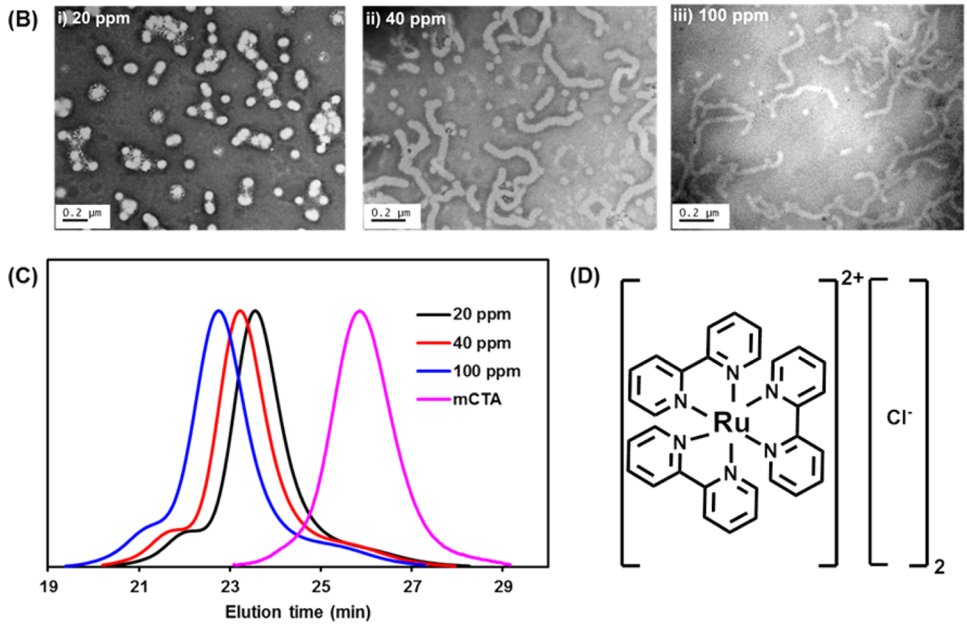

Figure 1. (A) Characterization of POEGMA-*b*-PBzMA diblock copolymers synthesized using (i) 20, (ii) 40, and (iii) 100 ppm catalyst relative to monomer concentration and a [BzMA]/[POEGMA] = 200:1; (B) TEM images of self-assembled POEGMA-*b*-PBzMA nanoparticles (Exp. i, ii, and iii); (C) GPC traces of POEGMA-*b*-PBzMA diblock copolymers (Exp. i, ii, and iii); (D) Chemical structure of the ruthenium-based photoredox catalyst used in this study.

(A)

Exp.	Total solids content (wt%)	Conversion (%)	$M_{n,\,theo}$ (g/mol)	$M_{n,\,NMR}$ (g/mol)	$M_{n,\,GPC}$ (g/mol)	Đ	D_h (DLS) (nm)	DLS PDI
iv	10	68	32 900	30 700	26 700	1.23	153	0.19
v	15	76	35 800	43 000	31 200	1.29	385	0.22
vi	20	72	34 400	32 300	27 800	1.22	Colloidially unstable	

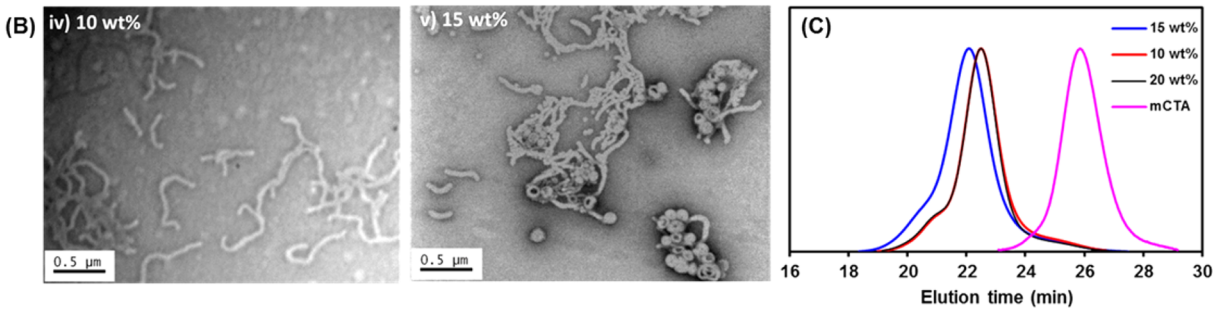

Figure 2. (A) Characterization of POEGMA-*b*-PBzMA diblock copolymers synthesized at a total solids content of (iv) 10, (v) 15, and (vi) 20 wt % and a [BzMA]/[POEGMA] = 200:1; (B) TEM images of self-assembled POEGMA-*b*-PBzMA nanoparticles (Exp. iv, v); and (C) GPC traces of POEGMA-*b*-PBzMA diblock copolymers (Exp. iv, v, and vi).

these unreacted chains could be attributed to poor reinitiation of homopolymer chains in dispersed media during the PISA process and "dead" homopolymer chains produced during the synthesis of the homopolymer using conventional RAFT

DOI: 10.1021/acsmacrolett.5b00523
ACS Macro Lett. 2015, 4, 984−990

(A)

Exp.	Total solids content (wt%)	MeCN content (%)	Conversion (%)	$M_{n,theo}$ (g/mol)	$M_{n,NMR}$ (g/mol)	$M_{n,GPC}$ (g/mol)	Đ	D_h (DLS) (nm)	DLS PDI
vii	10	0	60	30 100	28 700	24 900	1.24	184	0.23
viii	10	10	61	30 500	29 300	25 000	1.23	490	0.28
ix	20	20	68	33 000	31 400	29 500	1.20	734	0.28

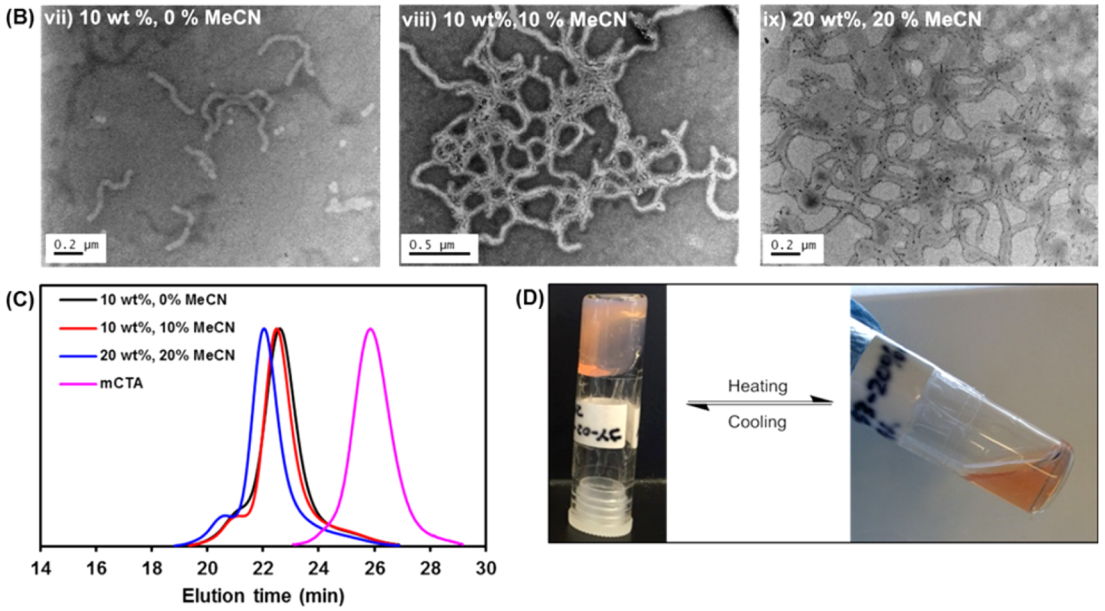

Figure 3. (A) Characterization of POEGMA-*b*-PBzMA diblock copolymers synthesized using (vii) 10 wt % solid content, 0 v/v % MeCN; (viii) 10 wt % solid content, 10 v/v % MeCN; and (ix) 20 wt % solid content, 20 v/v % MeCN and a [BzMA]/[POEGMA] = 200:1; (B) TEM images of self-assembled POEGMA-*b*-PBzMA nanoparticles (Exp. vii, viii, and ix) and (C) GPC traces of POEGMA-*b*-PBzMA diblock copolymers (Exp. vii, viii, and ix). (D) Digital photos depicting a reversible transition from a free-standing gel-like state to a free-flowing dispersion upon heating.

polymerization. UV analysis revealed the presence of shoulder at low retention time, which could be attributed to "unreacted" polymers. Furthermore, to investigate the living character of the polymerization, a model kinetic study was performed using a POEGMA macroinitiator (POEGMA-2, SI, Table S1) which exhibits a linear increase in $M_{n,GPC}$ and slight increase in polymer dispersity (M_w/M_n < 1.3) with monomer conversion (SI, Figure S5). Furthermore, $M_{n,GPC}$ are in good agreement with theoretical values. During the dispersion polymerizations, the solutions gradually became cloudy, indicating the formation of dispersed particles due to the aggregation of the insoluble PBzMA block. Transmission electron microscope (TEM) images of these particles indicated that a morphological transition from spheres (Exp. **i**) to mixtures of spheres and short worm-like micelles (Exp. **ii** and **iii**) occurred as the catalyst concentration (and conversion) increased (Figure 1B). This observation of increasing particle size was also supported by dynamic light scattering (DLS) data (Figure 1A, SI, Figure S6A), which although generally only applicable for spherical particles, can be used to provide an indication of morphological evolution, as reported by Armes and other groups.[6g,7a,20,22] This initial study demonstrated the feasibility of the PET-RAFT polymerization of BzMA to drive the PISA process in ethanolic solution. In subsequent PISA experiments, 100 ppm of catalyst relative to monomer concentration was employed to obtain a reasonable polymerization rate as well as good control over the molecular weight distribution.

In order to determine whether higher order morphologies could be formed within 24 h, we varied the total solids content of the reaction, while maintaining a [BzMA]/[POEGMA] = 200:1. An increase in the total solids content was expected to increase both the polymerization rate and interparticle interactions favoring morphological evolution. PET-RAFT dispersion polymerizations were conducted at 10, 15, and 20 wt % solids content for 24 h with a gradual increase in turbidity observed during the polymerization. After 24 h, stable suspensions were obtained, except that macroscopic precipitation was observed for Exp vi, which was attributed to the rapid polymerization of BzMA inhibiting nanoparticle rearrangement and, hence, leading to colloidal instability. In all cases, control over the polymerization was maintained as demonstrated by low dispersities (M_w/M_n > 1.3; Figure 2A,C).

TEM images revealed that increasing the solids contents to 15 wt % led to the formation of a morphology mixture with three phases (spherical micelles, worm-like micelles, and vesicles) within a single formulation (Figure 2B). The presence of a mixed morphology has previously been reported[4c,23] and can be partially attributed to the poor mobility of the core-forming polymer chains in the reaction medium. It is suggested that this effect is less pronounced in thermally initiated PISA systems because they are mostly conducted above the glass transition temperature (T_g) of the core-forming polymer.[24] Since the PET-RAFT PISA of BzMA is performed at room temperature (below the T_g of the PBzMA homopolymer), the limited core mobility leads to uneven morphological evolution of the nanoparticle shape. As a result, stabilization of the intermediate worm-like micelle phase to obtain a pure morphology may be difficult. Apart from increasing the

DOI: 10.1021/acsmacrolett.5b00523
ACS Macro Lett. 2015, 4, 984−990

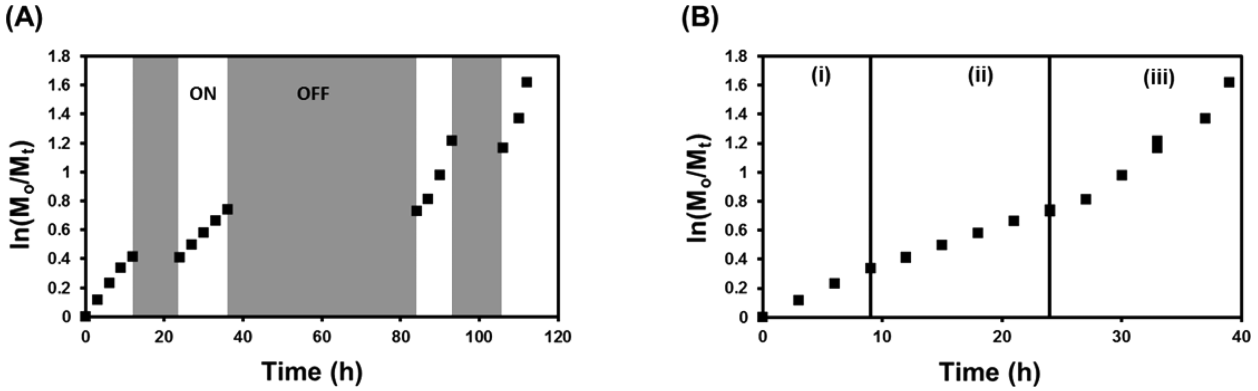

Figure 4. (A) "ON/OFF" kinetics of PET-RAFT PISA monitored by online FTNIR. (B) Kinetics adjusted for total irradiation time by removing the OFF periods.

polymerization temperature, the addition of plasticizing solvents to swell the core block has also been proposed. Therefore, to test our hypothesis, we introduced a small volume fraction of acetonitrile (MeCN) into the reaction medium.

Interestingly, the addition of 10 v/v % MeCN to a polymerization conducted at 10 wt % solids content had little effect on both the overall polymerization rate of BzMA (60% vs 61% monomer conversion in Exp. vii and viii, respectively, Figure 3A) and the control of the polymerization as indicated by GPC traces (Figure 3C). However, we observed different rheological behavior between Exp. vii and viii, whereby Exp. viii underwent a gradual increase in viscosity during the polymerization. After 24 h, the dispersion had formed a highly viscous solution, which could be reversibly transformed to a free-flowing solution when heated at ~70 °C. Alternatively, dilution with EtOH also resulted in a stable free-flowing dispersion indicating that the gel-like behavior was not due to a typical Trommsdorff autoacceleration effect.[25] Furthermore, the nanoparticles could be readily dissolved in organic solvents, such as chloroform or *N*,*N*-dimethylacetamide. TEM examination revealed the exclusive formation of worm-like micelles, which have previously been reported to give rise to macroscopic gelation behavior due to strong interworm entanglements.[26] However, the syntheses of these gels are normally performed using a thermally initiated PISA process such that macroscopic gelation is not observed until the reaction is quenched to room temperature (which may be a result of a sphere-to-worm morphology transition). By polymerizing below the gelation temperature, the occurrence of in situ gelation allows us to readily isolate pure worm-like micelles by monitoring the increase in solution viscosity. Furthermore, the addition of 20 v/v % MeCN to a polymerization mixture at 20 wt % solid content (Exp. ix) resulted in the formation of a free-standing gel after 24 h. TEM images revealed the formation of worm-like micelles resulting in the formation of macroscopic gels that undergo thermoreversible gelation (Figure 3B,D). Interestingly, longer irradiation time of these gels leads to macroscopic precipitation rather than a vesicle morphology as is typically observed in a thermally initiated PISA process. This is likely due to the high viscosity of the dispersion inhibiting further nanoparticle rearrangement to a vesicle phase. This behavior provides a useful means to specifically isolate worm-like phases due to the in situ system gelation suppressing further morphological evolution.

We have previously demonstrated the high degree of temporal control that exists in homogeneous PET-RAFT polymerizations.[15b,16] To examine whether the PET-RAFT PISA system can be temporally controlled, we exposed the polymerization mixture to alternating "ON/OFF" periods of external light stimulation. The polymerization kinetics were readily monitored by online Fourier transform near-infrared (FTNIR) spectroscopy in which the disappearance of the monomeric vinyl absorption (~6100 cm^{-1}) is related quantitatively to monomer conversion. In addition, UV−vis spectra were acquired at different time points in order to monitor changes in absorbance (scattering) caused by nanoparticle formation during the dispersion polymerization. Using a POEGMA macro-CTA with a slightly higher DP (POEGMA-2, SI, Table S1 $M_{n,NMR}$ = 10050 g mol^{-1} and $Đ$ = 1.13), an "ON/OFF" experiment was conducted using 100 ppm of catalyst relative to monomer concentration and [BzMA]/[POEGMA] = 200:1. In order to increase the absolute intensity of the vinylic signal, polymerizations were conducted at 20 wt % solids content with 20 v/v % MeCN to aid in stabilizing the worm-like micelles. Figure 4A indicates that when the external light source is OFF, monomer consumption is halted; conversely, with the light ON, monomer consumption is resumed (Figure 4). In contrast to the linear kinetic plots in homogeneous PET-RAFT systems,[15b,16] an unexpected nonlinear evolution of $\ln([M]_0/[M]_t)$ was observed in our PET-RAFT PISA system, which is attributed to particle nucleation and morphology evolution. Interestingly, after a total of 39 h of irradiation with visible light, a free-standing gel was formed (SI, Figure S7B). TEM images indicated the formation of highly branched worm-like micelles suggesting that morphology control was still possible despite the intermittent application of the light stimulus (SI, Figure S7A).

By plotting $\ln([M]_0/[M]_t)$ versus the total irradiation time (i.e., removing the OFF periods), we could observe three polymerization phases (Figure 4B). In the early phase, $\ln([M]_0/[M]_t)$ increased fairly linearly with time, which is attributed to the initially homogeneous reaction mixture (k_p^{app} = 0.0375 h^{-1}). When the PBzMA block exceeded a critical degree of polymerization, initial micellization occurred, resulting in a change in turbidity. As a result, penetration of visible light through the turbid medium was restricted which could cause a slight slowing of the polymerization rate in the second polymerization phase (k_p^{app} = 0.0273 h^{-1}). This change in polymerization rates coincided with an increase in the apparent absorption of visible light by the reaction mixture measured by UV−visible spectroscopy (SI, Figure S8). At around 30% monomer conversion, the absorbance started to

DOI: 10.1021/acsmacrolett.5b00523
ACS Macro Lett. 2015, 4, 984−990

increase gradually which concurred with a slowdown of the polymerization. Finally, as the heterogeneous polymerization continued, the increasing number of entanglements from the formation of worm-like micelles could cause an increase in the reaction viscosity and hence acceleration of the polymerization rate (k_p^{app} = 0.0561 h^{-1}). This promoted the evolution of the worm-like phase, further increasing the viscosity, which could cause autoacceleration type effects. It is interestingly to note that the copolymers obtained during the gel formation presented a relatively low dispersity (<1.30).

In conclusion, we have successfully demonstrated the application of visible light-mediated PET-RAFT polymerization in a PISA dispersion process. Manipulation of intrinsic reaction parameters was used to generate nanoparticles of different morphologies, such as spherical-, worm-like micelles and vesicles. We have found that by polymerizing at room temperature, formation of highly pure worm-like micelles leads to in situ gelation of the reaction mixture, providing a useful method to isolate this intermediate morphology. The ability to reproducibly generate pure worm-like micelles is expected to have important implications for potential applications in drug delivery. Finally, online FTNIR measurements have demonstrated that the photoredox catalyzed PISA process can be temporally controlled simply by modulating the light ON and OFF.

■ ASSOCIATED CONTENT

Supporting Information

Experimental details, NMR spectra, DLS results (Figures S1–S8 and Table S1). The Supporting Information is available free of charge on the ACS Publications website at DOI: 10.1021/acsmacrolett.5b00523.

(PDF)

■ AUTHOR INFORMATION

Corresponding Author

*E-mail: cboyer@unsw.edu.au.

Notes

The authors declare no competing financial interest.

■ ACKNOWLEDGMENTS

The authors thank UNSW Mark Wainwright Analytical Center. C.B. acknowledges the Australian Research Council (ARC) for his Future Fellowship (FT12010096) and UNSW for funding.

■ REFERENCES

(1) (a) Thompson, K. L.; Fielding, L. A.; Mykhaylyk, O. O.; Lane, J. A.; Derry, M. J.; Armes, S. P. *Chem. Sci.* **2015**, *6*, 4207–4214. (b) Mai, Y.; Eisenberg, A. *Chem. Soc. Rev.* **2012**, *41*, 5969–5985. (c) Warren, N. J.; Armes, S. P. *J. Am. Chem. Soc.* **2014**, *136*, 10174–10185. (d) Li, Y.; Jiang, T.; Lin, S.; Lin, J.; Cai, C.; Zhu, X. *Sci. Rep.* **2015**, *5*, 10137. (e) van Dongen, S. F. M.; de Hoog, H.-P. M.; Peters, R. J. R. W.; Nallani, M.; Nolte, R. J. M.; van Hest, J. C. M. *Chem. Rev.* **2009**, *109*, 6212–6274. (f) Nasiri, M.; Bertrand, A.; Reineke, T. M.; Hillmyer, M. A. *ACS Appl. Mater. Interfaces* **2014**, *6*, 16283–16288. (g) Yin, L.; Dalsin, M. C.; Sizovs, A.; Reineke, T. M.; Hillmyer, M. A. *Macromolecules* **2012**, *45*, 4322–4332.

(2) (a) Rodríguez-Hernández, J.; Chécot, F.; Gnanou, Y.; Lecommandoux, S. *Prog. Polym. Sci.* **2005**, *30*, 691–724. (b) Riess, G. *Prog. Polym. Sci.* **2003**, *28*, 1107–1170.

(3) Zhang, L.; Eisenberg, A. *Science* **1995**, *268*, 1728–1731.

(4) (a) Jain, S.; Bates, F. S. *Science* **2003**, *300*, 460–464. (b) Dong, S.; Zhao, W.; Lucien, F. P.; Perrier, S.; Zetterlund, P. B. *Polym. Chem.* **2015**, *6*, 2249–2254. (c) Blanazs, A.; Ryan, A. J.; Armes, S. P. *Macromolecules* **2012**, *45*, 5099–5107.

(5) Zhang, L.; Yu, K.; Eisenberg, A. *Science* **1996**, *272*, 1777–1779.

(6) (a) Yang, P.; Ratcliffe, L. P. D.; Armes, S. P. *Macromolecules* **2013**, *46*, 8545–8556. (b) Chambon, P.; Blanazs, A.; Battaglia, G.; Armes, S. P. *Macromolecules* **2012**, *45*, 5081–5090. (c) He, W.-D.; Sun, X.-L.; Wan, W.-M.; Pan, C.-Y. *Macromolecules* **2011**, *44*, 3358–3365. (d) Wan, W.-M.; Pan, C.-Y. *Polym. Chem.* **2010**, *1*, 1475–1484. (e) Kang, Y.; Pitto-Barry, A.; Maitland, A.; O'Reilly, R. K. *Polym. Chem.* **2015**, *6*, 4984–4992. (f) Zhou, W.; Qu, Q.; Yu, W.; An, Z. *ACS Macro Lett.* **2014**, *3*, 1220–1224. (g) Karagoz, B.; Esser, L.; Duong, H. T.; Basuki, J. S.; Boyer, C.; Davis, T. P. *Polym. Chem.* **2014**, *5*, 350–355. (h) Karagoz, B.; Yeow, J.; Esser, L.; Prakash, S. M.; Kuchel, R. P.; Davis, T. P.; Boyer, C. *Langmuir* **2014**, *30*, 10493–10502. (i) Zhou, W.; Qu, Q.; Xu, Y.; An, Z. *ACS Macro Lett.* **2015**, *4*, 495–499. (j) Bleach, R.; Karagoz, B.; Prakash, S. M.; Davis, T. P.; Boyer, C. *ACS Macro Lett.* **2014**, *3*, 591–596. (k) An, Z.; Shi, Q.; Tang, W.; Tsung, C.-K.; Hawker, C. J.; Stucky, G. D. *J. Am. Chem. Soc.* **2007**, *129*, 14493–14499. (l) Hou, L.; Ma, K.; An, Z.; Wu, P. *Macromolecules* **2014**, *47*, 1144–1154. (m) Charleux, B.; Delaittre, G.; Rieger, J.; D'Agosto, F. *Macromolecules* **2012**, *45*, 6753–6765. (n) Zhang, Q.; Zhu, S. *ACS Macro Lett.* **2015**, *4*, 755–758. (o) Li, S.; He, X.; Li, Q.; Shi, P.; Zhang, W. *ACS Macro Lett.* **2014**, *3*, 916–921. (p) Shi, P.; Zhou, H.; Gao, C.; Wang, S.; Sun, P.; Zhang, W. *Polym. Chem.* **2015**, *6*, 4911–4920. (q) Gao, C.; Li, S.; Li, Q.; Shi, P.; Shah, S. A.; Zhang, W. *Polym. Chem.* **2014**, *5*, 6957–6966. (r) Dan, M.; Huo, F.; Xiao, X.; Su, Y.; Zhang, W. *Macromolecules* **2014**, *47*, 1360–1370.

(7) (a) Figg, C. A.; Simula, A.; Gebre, K. A.; Tucker, B. S.; Haddleton, D. M.; Sumerlin, B. S. *Chem. Sci.* **2015**, *6*, 1230–1236. (b) Rieger, J.; Grazon, C.; Charleux, B.; Alaimo, D.; Jérôme, C. *J. Polym. Sci., Part A: Polym. Chem.* **2009**, *47*, 2373–2390.

(8) Liu, G.; Qiu, Q.; Shen, W.; An, Z. *Macromolecules* **2011**, *44*, 5237–5245.

(9) (a) Yoshida, E. *Colloid Polym. Sci.* **2014**, *292*, 763–769. (b) Yoshida, E. *Colloid Polym. Sci.* **2015**, *293*, 249–256. (c) Yoshida, E. *Colloid Polym. Sci.* **2014**, *292*, 1463–1468. (d) Yoshida, E. *Colloid Polym. Sci.* **2015**, *293*, 649–653.

(10) (a) Tan, J.; Rao, X.; Wu, X.; Deng, H.; Yang, J.; Zeng, Z. *Macromolecules* **2012**, *45*, 8790–8795. (b) Tan, J.; Rao, X.; Jiang, D.; Yang, J.; Zeng, Z. *Polymer* **2014**, *55*, 2380–2388.

(11) Liu, Z.; Zhang, G.; Lu, W.; Huang, Y.; Zhang, J.; Chen, T. *Polym. Chem.* **2015**, *6*, 6129–6132.

(12) (a) Chen, M.; Johnson, J. A. *Chem. Commun.* **2015**, *51*, 6742–6745. (b) Anastasaki, A.; Nikolaou, V.; Zhang, Q.; Burns, J.; Samanta, S. R.; Waldron, C.; Haddleton, A. J.; McHale, R.; Fox, D.; Percec, V.; Wilson, P.; Haddleton, D. M. *J. Am. Chem. Soc.* **2014**, *136*, 1141–1149. (c) Frick, E.; Anastasaki, A.; Haddleton, D. M.; Barner-Kowollik, C. *J. Am. Chem. Soc.* **2015**, *137*, 6889–6896. (d) Konkolewicz, D.; Schröder, K.; Buback, J.; Bernhard, S.; Matyjaszewski, K. *ACS Macro Lett.* **2012**, *1*, 1219–1223. (e) Ribelli, T. G.; Konkolewicz, D.; Bernhard, S.; Matyjaszewski, K. *J. Am. Chem. Soc.* **2014**, *136*, 13303–13312. (f) Tasdelen, M. A.; Uygun, M.; Yagci, Y. *Macromol. Chem. Phys.* **2010**, *211*, 2271–2275. (g) Tasdelen, M. A.; Çiftci, M.; Uygun, M.; Yagci, Y. *Progress in Controlled Radical Polymerization: Mechanisms and Techniques*; American Chemical Society: Washington, DC, 2012; Vol. *1100*, pp 59–72. (h) Ciftci, M.; Tasdelen, M. A.; Li, W.; Matyjaszewski, K.; Yagci, Y. *Macromolecules* **2013**, *46*, 9537–9543. (i) Shi, Y.; Liu, G.; Gao, H.; Lu, L.; Cai, Y. *Macromolecules* **2009**, *42*, 3917–3926. (j) Liu, G.; Shi, H.; Cui, Y.; Tong, J.; Zhao, Y.; Wang, D.; Cai, Y. *Polym. Chem.* **2013**, *4*, 1176–1182. (k) McKenzie, T. G.; Fu, Q.; Wong, E. H. H.; Dunstan, D. E.; Qiao, G. G. *Macromolecules* **2015**, *48*, 3864–3872. (l) Ohtsuki, A.; Lei, L.; Tanishima, M.; Goto, A.; Kaji, H. *J. Am. Chem. Soc.* **2015**, *137*, 5610–5617. (m) Jiang, Y.; Xu, N.; Han, J.; Yu, Q.; Guo, L.; Gao, P.; Lu, X.; Cai, Y. *Polym. Chem.* **2015**, *6*, 4955–4965.

(13) (a) Fors, B. P.; Hawker, C. J. *Angew. Chem., Int. Ed.* **2012**, *51*, 8850–8853. (b) Treat, N. J.; Fors, B. P.; Kramer, J. W.; Christianson, M.; Chiu, C.-Y.; Alaniz, J. R. d.; Hawker, C. J. *ACS Macro Lett.* **2014**, *3*, 580–584. (c) Yang, Q.; Dumur, F.; Morlet-Savary, F.; Poly, J.; Lalevée,

DOI: 10.1021/acsmacrolett.5b00523
ACS Macro Lett. 2015, 4, 984–990

J. *Macromolecules* **2015**, *48*, 1972−1980. (d) Mosnáček, J.; Ilčíková, M. t. *Macromolecules* **2012**, *45*, 5859−5865. (e) Pan, X.; Lamson, M.; Yan, J.; Matyjaszewski, K. *ACS Macro Lett.* **2015**, *4*, 192−196.
(14) Ogawa, K. A.; Goetz, A. E.; Boydston, A. J. *J. Am. Chem. Soc.* **2015**, *137*, 1400−1403.
(15) (a) Xu, J.; Jung, K.; Atme, A.; Shanmugam, S.; Boyer, C. *J. Am. Chem. Soc.* **2014**, *136*, 5508−5519. (b) Xu, J.; Jung, K.; Boyer, C. *Macromolecules* **2014**, *47*, 4217−4229. (c) Chen, M.; MacLeod, M. J.; Johnson, J. A. *ACS Macro Lett.* **2015**, *4*, 566−569. (d) Shanmugam, S.; Xu, J.; Boyer, C. *J. Am. Chem. Soc.* **2015**, *137*, 9174−9185. (e) Shanmugam, S.; Xu, J.; Boyer, C. *Chem. Sci.* **2015**, *6*, 1341−1349. (f) Shanmugam, S.; Boyer, C. *J. Am. Chem. Soc.* **2015**, *137* (31), 9988−9999.
(16) Shanmugam, S.; Xu, J.; Boyer, C. *Macromolecules* **2014**, *47*, 4930−4942.
(17) (a) Jones, E. R.; Semsarilar, M.; Blanazs, A.; Armes, S. P. *Macromolecules* **2012**, *45*, 5091−5098. (b) Semsarilar, M.; Jones, E. R.; Blanazs, A.; Armes, S. P. *Adv. Mater.* **2012**, *24*, 3378−3382.
(18) Xu, J.; Shanmugam, S.; Duong, H. T.; Boyer, C. *Polym. Chem.* **2015**, *6*, 5615−5624.
(19) Xu, J.; Jung, K.; Corrigan, N. A.; Boyer, C. *Chem. Sci.* **2014**, *5*, 3568−3575.
(20) Pei, Y.; Lowe, A. B. *Polym. Chem.* **2014**, *5*, 2342−2351.
(21) (a) Boyer, C.; Soeriyadi, A. H.; Zetterlund, P. B.; Whittaker, M. R. *Macromolecules* **2011**, *44*, 8028−8033. (b) Gody, G.; Maschmeyer, T.; Zetterlund, P. B.; Perrier, S. *Macromolecules* **2014**, *47*, 639−649. (c) Gilbert, R. G. *Trends Polym. Sci.* **1995**, *3*, 222−226.
(22) (a) Semsarilar, M.; Penfold, N. J. W.; Jones, E. R.; Armes, S. P. *Polym. Chem.* **2015**, *6*, 1751−1757. (b) Fielding, L. A.; Derry, M. J.; Ladmiral, V.; Rosselgong, J.; Rodrigues, A. M.; Ratcliffe, L. P. D.; Sugihara, S.; Armes, S. P. *Chem. Sci.* **2013**, *4*, 2081−2087.
(23) Derry, M. J.; Fielding, L. A.; Armes, S. P. *Polym. Chem.* **2015**, *6*, 3054−3062.
(24) Blanazs, A.; Madsen, J.; Battaglia, G.; Ryan, A. J.; Armes, S. P. *J. Am. Chem. Soc.* **2011**, *133*, 16581−16587.
(25) Trommsdorff, V. E.; Köhle, H.; Lagally, P. *Makromol. Chem.* **1948**, *1*, 169−198.
(26) Fielding, L. A.; Lane, J. A.; Derry, M. J.; Mykhaylyk, O. O.; Armes, S. P. *J. Am. Chem. Soc.* **2014**, *136*, 5790−5798.

NOTE ADDED AFTER ASAP PUBLICATION

This paper was published ASAP on August 27, 2015 with errors to the text and a reference. The corrected version was republished on August 31, 2015.

DOI: 10.1021/acsmacrolett.5b00523
ACS Macro Lett. 2015, 4, 984−990